

This is a repository copy of *Exploring Chemical Bonds through Variations in Magnetic Shielding*.

White Rose Research Online URL for this paper:  
<http://eprints.whiterose.ac.uk/95553/>

Version: Accepted Version

---

**Article:**

Karadakov, Peter Borislavov [orcid.org/0000-0002-2673-6804](http://orcid.org/0000-0002-2673-6804) and Horner, Kate Elizabeth (2016) Exploring Chemical Bonds through Variations in Magnetic Shielding. *Journal of chemical theory and computation*. pp. 558-563. ISSN 1549-9618

<https://doi.org/10.1021/acs.jctc.5b00842>

---

**Reuse**

Items deposited in White Rose Research Online are protected by copyright, with all rights reserved unless indicated otherwise. They may be downloaded and/or printed for private study, or other acts as permitted by national copyright laws. The publisher or other rights holders may allow further reproduction and re-use of the full text version. This is indicated by the licence information on the White Rose Research Online record for the item.

**Takedown**

If you consider content in White Rose Research Online to be in breach of UK law, please notify us by emailing [eprints@whiterose.ac.uk](mailto:eprints@whiterose.ac.uk) including the URL of the record and the reason for the withdrawal request.

# Exploring Chemical Bonds through Variations in Magnetic Shielding

Peter B. Karadakov\* and Kate E. Horner

Department of Chemistry, University of York, Heslington, York, YO10 5DD, U.K.

**ABSTRACT:** Differences in nuclear isotropic magnetic shieldings give rise to the chemical shifts measured in NMR experiments. In contrast to existing NMR experimental techniques, quantum chemical methods are capable of calculating isotropic magnetic shieldings not just at nuclei, but also at any point in the space surrounding a molecule. Using *s-trans*-1,3-butadiene, ethane, ethene and ethyne as examples, we show that the variations in isotropic magnetic shielding around a molecule, represented as isosurfaces and contour plots, provide an unexpectedly clear picture of chemical bonding, which is much more detailed than the traditional description in terms of the total electron density.

## 1. INTRODUCTION

What would we see if we were able to measure magnetic shieldings not just at nuclei as in NMR spectroscopy, but also at any point within the space surrounding a molecule? Quantum chemical calculations reported in this paper indicate that we would observe a picture resembling the total electron density distribution coming from X-ray diffraction but, arguably, significantly richer in information about the nature of chemical bonds. Some of this additional information stems from the fact that an arbitrary point in space close to a molecule senses, through its magnetic shielding, the behavior of the electrons along all directions originating from this point, whereas the value of the total electron density at the same point does not carry much information about the density distribution in its surroundings, except for that expected of a smooth normalized function.

According to NMR theory, any nucleus  $J$  in a molecule subjected to an external magnetic field  $\mathbf{B}_0$  will “feel” a magnetic field  $\mathbf{B}_J$  which, in general, will not be the same as  $\mathbf{B}_0$ . For an isolated molecule, this is due to the shielding of nucleus  $J$  by the electrons in the molecule. Chemically different nuclei are surrounded by different electron environments and exhibit different extents of shielding.  $\mathbf{B}_J$  and  $\mathbf{B}_0$  are related through the equation

$$\mathbf{B}_J = (\mathbf{1} - \boldsymbol{\sigma}_J)\mathbf{B}_0$$

where  $\boldsymbol{\sigma}_J$  is the second-rank magnetic shielding tensor of nucleus  $J$ . The experimentally measured NMR chemical shift is equal to the difference between the isotropic shielding of a reference nucleus and the isotropic shielding of nucleus  $J$  (the isotropic shielding  $\sigma_{\text{iso}}$  is defined as one third of the trace of the shielding tensor).

In fact, not just nuclei, but also any point  $\mathbf{r}$  within the space surrounding a molecule at which there is some non-negligible electron density  $\rho(\mathbf{r})$  will be shielded and experience a magnetic field  $\mathbf{B}(\mathbf{r})$ , different from  $\mathbf{B}_0$ . The difference between  $\mathbf{B}(\mathbf{r})$  and  $\mathbf{B}_0$  can be used to define a magnetic shielding tensor at  $\mathbf{r}$ ,  $\boldsymbol{\sigma}(\mathbf{r})$ . At the moment, it is impossible to measure experimentally any of the characteristics of an off-nucleus shielding tensor, but this tensor can be evaluated in a straightforward manner using standard quantum chemical methods for calculating on-nucleus shielding tensors.

The first theoretical estimates of off-nucleus shieldings were obtained by Johnson and Bovey,<sup>1</sup> who developed a method for approximating ring current effects based on Pauling's free electron model and used it to calculate proton shieldings at different points in the surroundings of a benzene ring and construct a contour plot of "isoshielding" lines. Better-known examples of off-nucleus shieldings are provided by the different types of nucleus-independent chemical shift (NICS), popular aromaticity probes proposed by Schleyer and co-workers.<sup>2-6</sup>

Wolinski advanced the idea that the magnetic shielding tensor in an atom or molecule can be analyzed as a continuous function of the coordinates of a point in space and examined the changes in the shielding tensor  $\boldsymbol{\sigma}(\mathbf{r})$  along the molecular axis in a series of linear molecules.<sup>7</sup> He observed that, in general, the variations in the isotropic shielding  $\sigma_{\text{iso}}(\mathbf{r})$  and in the shielding components parallel and perpendicular to the molecular axis were similar to the behavior of the total electron density, but showed some differences which he attributed to the fact that the total electron density is responsible for the electron charge distribution, whereas magnetic properties, including shielding, are determined by the induced current density. The next major step in the theory of off-nucleus shieldings was the work of Kleinpeter *et al.*,<sup>8-11</sup> who generated isotropic chemical shielding surfaces (ICSSs) for a number of molecules using regular grids of  $\sigma_{\text{iso}}(\mathbf{r})$  values with a relatively wide spacing (0.5 Å). These ICSSs were then employed to discuss aromaticity and antiaromaticity, diatropic and paratropic regions within molecules, the anisotropic effects due to specific substituents, etc.

Isotropic shielding isosurfaces utilizing much denser regular grids of  $\sigma_{\text{iso}}(\mathbf{r})$  values (spacing of 0.05 Å) have been shown<sup>12-14</sup> to reveal subtle features of the isotropic shielding around a molecule which cannot be seen in the ICSSs of Kleinpeter and co-workers, constructed using coarser grids. These more detailed  $\sigma_{\text{iso}}(\mathbf{r})$  isosurfaces and contour plots allow very clear distinction between aromatic and antiaromatic systems, comparisons between the relative degrees of aromaticity of heterocycles with one and two heteroatoms, and highlight the extent to which chemical bonding is affected by aromaticity and antiaromaticity.

In this paper we analyze the possibility to describe chemical bonds using detailed computed isotropic shielding isosurfaces and contour plots. As the main example, we have chosen a molecule which is very familiar to chemists, *s-trans*-1,3-butadiene, an open-chain conjugated system containing formally single and double carbon-carbon bonds which, due to  $\pi$  electron delocalization, are stronger and weaker, respectively, than isolated carbon-carbon single and double bonds, such as those in ethane and ethene. To illustrate the difference between the single and double bonds in butadiene, a Hückel molecular orbital (HMO) calculation gives the corresponding total bond orders as 1.447 and 1.894, rather than 1 and 2, respectively. We show that the  $\sigma_{\text{iso}}(\mathbf{r})$  isosurfaces and contour plots distinguish between the two types of carbon-carbon bond in butadiene much better than the analogous total electron density plots; moreover, the isotropic shielding contour plots show visually discernible differences even between the rather similar symmetry-unique carbon-hydrogen bonds. The magnetic shielding picture of bonding in *s-trans*-1,3-butadiene is compared to analogous descriptions of bonding in molecules involving typical examples of carbon-carbon single, double and triple bonds, ethane, ethene and ethyne, respectively.

## 2. RESULTS AND DISCUSSION

All gas-phase isotropic magnetic shielding and total electron density values discussed in this paper were obtained using two methods, Hartree-Fock (HF) and second-order Møller-Plesset perturbation theory (MP2); when evaluating  $\sigma_{\text{iso}}(\mathbf{r})$  the molecular orbitals were expanded in terms of gauge-including atomic orbitals (GIAOs). All  $\sigma_{\text{iso}}(\mathbf{r})$  (HF-GIAO and MP2-GIAO) and  $\rho(\mathbf{r})$  (HF and MP2) calculations were performed within the 6-311++G(d,p) basis by means of GAUSSIAN09.<sup>15</sup> For *s-trans*-1,3-butadiene we used the  $C_{2h}$  gas-phase ground-state equilibrium geometry determined after adjusting the rotational constants obtained from rotational

spectroscopy by vibration-rotation constants coming from quantum chemical calculations;<sup>16</sup> for ethane, ethene and ethyne use was made of the respective  $D_{3d}$ ,  $D_{2h}$  and  $D_{\infty h}$  experimental geometries collected in Ref. 17. All calculations were carried out under the “SCF(Tight)” convergence criterion; the MP2 calculations were of the “MP2(Full)” type (accounting for all electrons in the correlation treatment); to increase the accuracy of the computed shielding tensors, HF-GIAO and MP2-GIAO calculations included the “CPHF(Separate)” keyword.

The three-dimensional grid of points employed in the construction of detailed  $\sigma_{\text{iso}}(\mathbf{r})$  and  $\rho(\mathbf{r})$  isosurfaces for *s-trans*-1,3-butadiene is defined within a right-handed Cartesian coordinate system with origin at the center of mass,  $z$  axis perpendicular to the molecular plane and  $y$  axis parallel to the two carbon-carbon “double” bonds. The grid is regular, in the shape of a cube centered at the origin of the coordinate system, with edges of 7 Å parallel to the  $x$ ,  $y$  and  $z$  axes, and spacing of 0.05 Å in each direction. To reduce computational effort,  $\sigma_{\text{iso}}(\mathbf{r})$  values were calculated only at the  $141 \times 71^2$  points within the first and second octants ( $y \geq 0, z \geq 0$ ); the remaining values were obtained through replication by symmetry. The grid points were specified in the GAUSSIAN09 input as ghost atoms without basis functions (symbol “Bq”); as the GAUSSIAN09 input routines limit the number of ghost atoms within a single geometry specification, it was necessary to perform 7482 separate NMR calculations. Each of these calculations included up to 95 ghost atoms and provided both HF-GIAO and MP2-GIAO results. The set of input files was prepared by means of a purpose-written program. For visualization purposes, all  $141^3$  HF-GIAO and MP2-GIAO  $\sigma_{\text{iso}}(\mathbf{r})$  values obtained for *s-trans*-1,3-butadiene were assembled in GAUSSIAN cube files.<sup>18</sup> GAUSSIAN cube files of HF and MP2  $\rho(\mathbf{r})$  values were generated directly by means of the GAUSSIAN cubegen utility.

The  $\sigma_{\text{iso}}(\mathbf{r})$  and  $\rho(\mathbf{r})$  isosurfaces and contour plots for *s-trans*-1,3-butadiene, and the  $\sigma_{\text{iso}}(\mathbf{r})$  contour plots for ethane, ethene and ethyne (*vide infra*), obtained using the HF and MP2 methods turned out to be very similar; therefore, we show and discuss the MP2 results only.



**Figure 1.** MP2-GIAO isotropic shielding (a) and MP2 total electron density (b) isosurfaces for *s-trans*-1,3-butadiene. (a)  $\sigma_{\text{iso}}(\mathbf{r}) = \pm 16$  ppm, positive and negative  $\sigma_{\text{iso}}(\mathbf{r})$  values are shown in blue and red, the  $\sigma_{\text{iso}}(\mathbf{r}) = -16$  ppm values form four oval shapes, surrounding the carbons. (b)  $\rho(\mathbf{r}) = 0.1$  a.u.

The  $\sigma_{\text{iso}}(\mathbf{r}) = \pm 16$  ppm and  $\rho(\mathbf{r}) = 0.1$  a.u. isosurfaces for *s-trans*-1,3-butadiene are shown in Figure 1. While, superficially, the isotropic shielding and total electron density isosurfaces look similar, there are several notable differences. The bulges over the C–C “double” bonds on the  $\sigma_{\text{iso}}(\mathbf{r}) = 16$  ppm isosurface are noticeably larger than that over the “single” bond in the middle. In contrast, the  $\rho(\mathbf{r}) = 0.1$  a.u. isosurface envelops both “double” and “single” C–C bonds in very much the same manner and does not allow visual differentiation between the two types of bond. The  $\sigma_{\text{iso}}(\mathbf{r}) = -16$  ppm isosurface (shown in red in Figure 1) illustrates the presence of relatively small deshielded regions around the carbon atoms. Such deshielded regions around  $\text{sp}^2$  hybridized second-row atoms have been observed previously<sup>12–14</sup> and it was thought that their most likely cause were ring currents associated with the  $\pi$  electrons. However, *s-trans*-1,3-butadiene is an open-chain conjugated system devoid of traditional ring currents. The presence of deshielded “halos” around  $\text{sp}^2$  hybridized carbons in *s-trans*-1,3-butadiene suggests that this effect is associated with a specific type of  $\pi$  electron motion, localized around  $\text{sp}^2$  hybridized second-row atoms and different from traditional ring currents.

There is a certain similarity between the  $\sigma_{\text{iso}}(\mathbf{r}) = \pm 16$  ppm MP2-GIAO/6-311++G(d,p) isosurface for *s-trans*-1,3-butadiene shown in Figure 1 and the  $\sigma_{\text{iso}}(\mathbf{r}) = \pm 16$  ppm CASSCF(6,6)-GIAO/6-311++G(d,p) (complete active-space self-consistent field with “6 electrons in 6 orbitals”) isosurface for benzene reported in Ref. 12, especially in the regions surrounding C–H bonds [as it was found in Ref. 12, in the case of benzene the HF-GIAO, MP2-GIAO and CASSCF(6,6)-GIAO methods, all in the 6-311++G(d,p) basis, produce very similar shielding pictures]. The proximity, on the inside of the benzene ring, of the shielded regions surrounding

C–C bonds in benzene makes these horizontally wider than the corresponding regions in *s-trans*-1,3-butadiene; however, the vertical extents of the C–C bonds in benzene are between those of C–C “double” and “single” bonds in *s-trans*-1,3-butadiene, which reflects the well-known differences in the strengths of these bonds (for example, the total HMO bond order for a C–C bond in benzene is 1.667, between the respective values for the C–C bonds in butadiene, see the Introduction).

To provide more detailed pictures of the changes in the isotropic shielding and total electron density around *s-trans*-1,3-butadiene, we prepared  $\sigma_{\text{iso}}(\mathbf{r})$  and  $\rho(\mathbf{r})$  contour plots in four planes (see Figures 2–5): The molecular plane  $\sigma_{\text{h}}$ , a composite vertical plane  $\sigma_{\parallel}$  passing through all three carbon-carbon bonds and perpendicular to the molecular plane, and two vertical planes perpendicular to the “double” and “single” carbon-carbon bonds,  $\sigma_{\perp\text{d}}$  and  $\sigma_{\perp\text{s}}$ , each of which slices the respective bond in half. Data for the  $\sigma_{\text{h}}$  contour plots were extracted from the respective three-dimensional  $\sigma_{\text{iso}}(\mathbf{r})$  and  $\rho(\mathbf{r})$  grids; values used in the construction of the remaining contour plots were calculated independently, using appropriate two-dimensional grids of points with spacing of 0.05 Å in each direction.

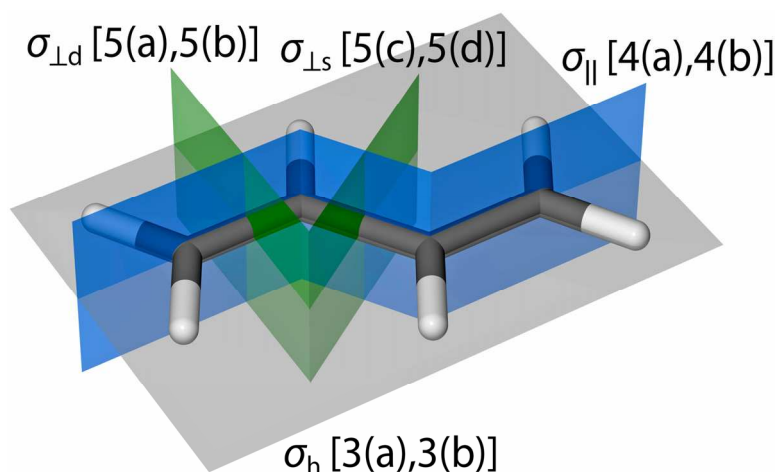


**Figure 2.** Planes in *s-trans*-1,3-butadiene. Molecular plane  $\sigma_{\text{h}}$  (grey, used in Figure 3); composite vertical plane  $\sigma_{\parallel}$  passing through all three carbon-carbon bonds and perpendicular to  $\sigma_{\text{h}}$  (blue, includes three plane segments, each of which slices through one carbon-carbon bond, used in Figure 4);  $\sigma_{\perp\text{d}}$  and  $\sigma_{\perp\text{s}}$  vertical planes perpendicular to the “double” and “single” carbon-carbon bonds, each plane passes through the midpoint of the respective bond (green, used in Figure 5).

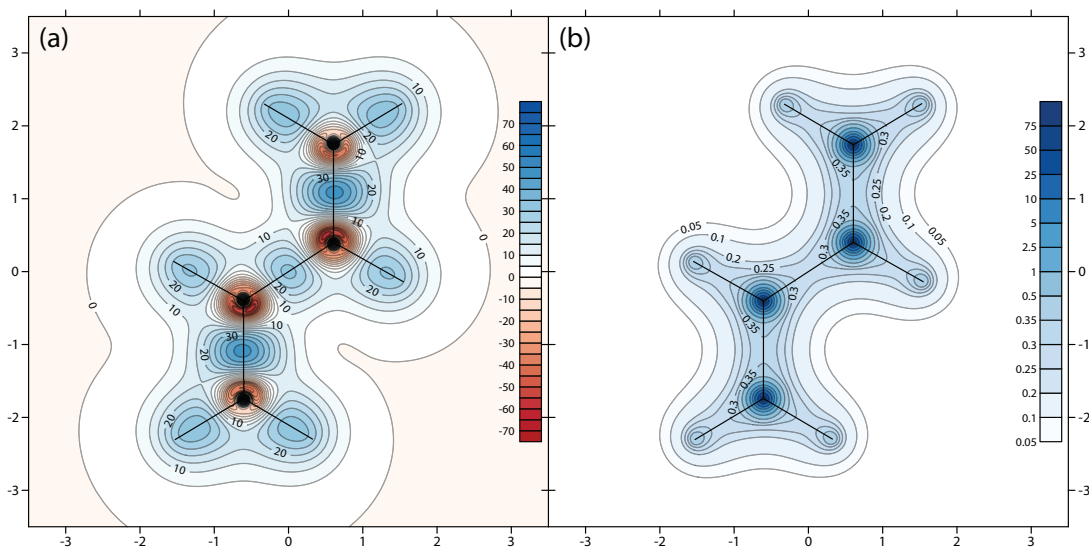


**Figure 3.** MP2-GIAO isotropic shielding (a) and MP2 total electron density (b) contour plots for *s-trans*-1,3-butadiene in the molecular plane  $\sigma_h$  (see Figure 2).  $\sigma_{\text{iso}}(\mathbf{r})$  in ppm,  $\rho(\mathbf{r})$  in a.u., distances in Å.

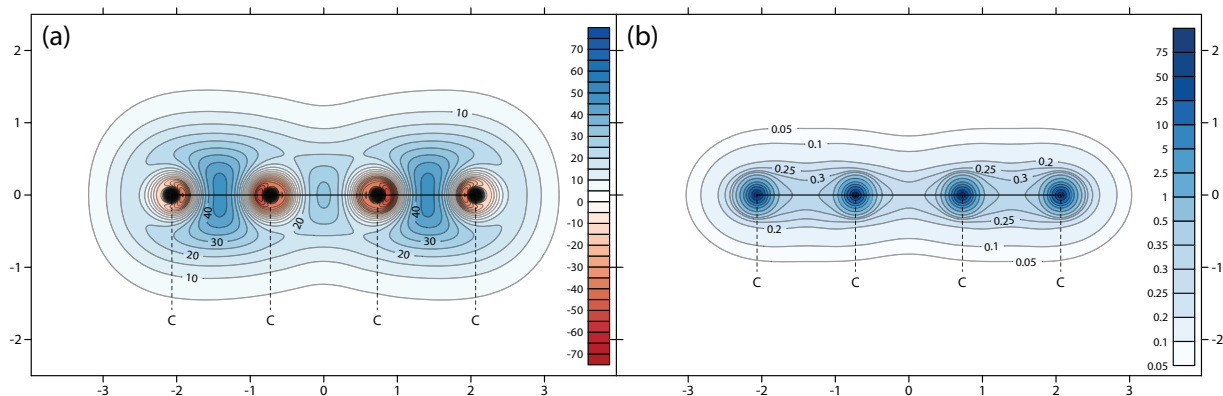


**Figure 4.** MP2-GIAO isotropic shielding (a) and MP2 total electron density (b) contour plots for *s-trans*-1,3-butadiene in the composite vertical plane  $\sigma_{\parallel}$  (see Figure 2).  $\sigma_{\text{iso}}(\mathbf{r})$  in ppm,  $\rho(\mathbf{r})$  in a.u., distances in Å, dotted lines specify the positions of the carbons.

The comparison between the  $\sigma_{\text{iso}}(\mathbf{r})$  and  $\rho(\mathbf{r})$  contour plots in the  $\sigma_h$  and  $\sigma_{\parallel}$  planes (see Figures 3 and 4) reveals further important differences between these quantities. When moving along a bond, away from an atom, the total electron density rapidly decreases and reaches a minimum at or close to the bond midpoint (or a bit closer to the H atom, for C–H bonds). Chemical intuition suggests that the isotropic shielding should behave in a similar way and areas surrounded by higher electronic density would be more shielded than areas surrounded by lower

electronic density. However, the off-nucleus isotropic shielding follows a different pattern: When moving along a bond and away from an  $sp^2$  hybridized carbon atom, initially the isotropic shielding falls sharply and becomes negative, then once past the deshielded region surrounding the atom it starts to increase and reaches a maximum at or very close to the bond midpoint. If we start at a hydrogen atom, the isotropic shielding increases all the way to the central part of the bond. Figure 3(a), which shows the horizontal cross sections of all C–C and C–H bonds in *s-trans*-1,3-butadiene, and Figures 4(a), 5(a) and 5(c), which show the vertical cross sections of the C–C bonds, clearly demonstrate the presence of sizeable shielded regions enveloping individual bonds; stronger bonds are inside larger shielded regions, within which both the rate at which the shielding increases when approaching the line connecting the atoms and the maximum shielding achieved are higher than those for weaker bonds. While a careful analysis of the total electron density contour plots [see Figures 3(b), 4(b), 5(b) and 5(d)] can also reveal some differences between stronger and weaker bonds, these differences are more subtle and much less obvious than the differences observed in the isotropic shielding contour plots.

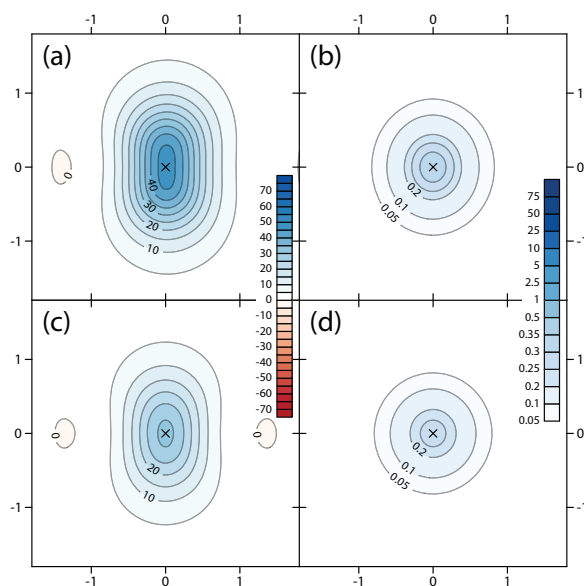


**Figure 5.** MP2-GIAO isotropic shielding (a,c) and MP2 total electron density (b,d) contour plots for *s-trans*-1,3-butadiene in the  $\sigma_{\perp d}$  (a,b) and  $\sigma_{\perp s}$  (c,d) vertical planes perpendicular to the “double” and “single” carbon-carbon bonds (see Figure 2).  $\sigma_{\text{iso}}(r)$  in ppm,  $\rho(r)$  in a.u., distances in Å, crosses specify the positions of the bonds.

When examining the isotropic shielding and total electron density contour plots in the molecular plane [see Figure 3, (a) and (b)] it is important to realize that the in-plane  $\sigma_{\text{iso}}(\mathbf{r})$  values include  $\pi$  electron contributions, coming from  $\sigma_{zz}(\mathbf{r})$ , whereas the in-plane  $\rho(\mathbf{r})$  is determined entirely by the  $\sigma$  electrons. This is one of the reasons why the bonding picture shown by the  $\sigma_{\text{iso}}(\mathbf{r})$  contour plot in Figure 3(a) is more featureful in comparison to its  $\rho(\mathbf{r})$  counterpart in Figure 3(b). However, even though the total electron density plots in vertical planes in Figures 4(b), 5(b) and 5(d) include both  $\sigma$  and  $\pi$  electron contributions, the differences between “single” and “double” C–C bonds are much easier to observe in the corresponding isotropic shielding contour plots in Figures 4(a), 5(a) and 5(c), respectively.

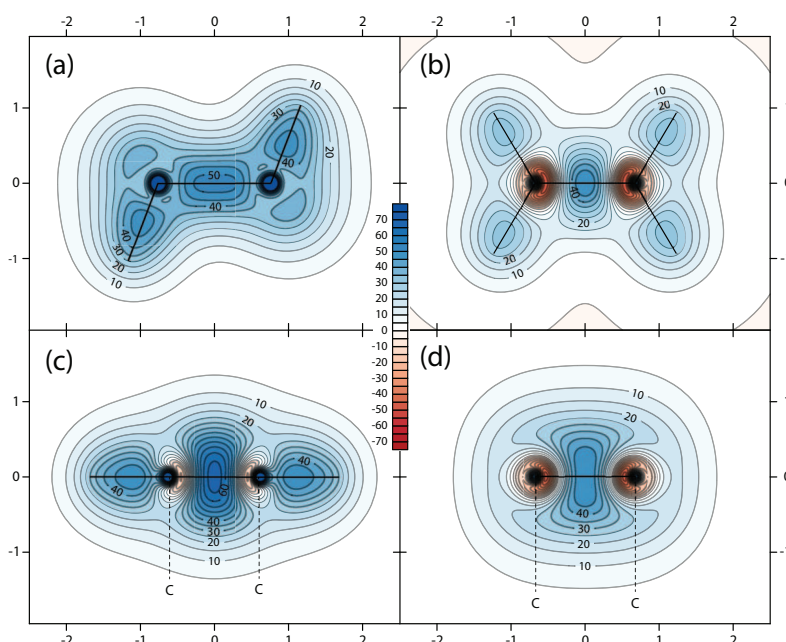


**Figure 6.** MP2-GIAO isotropic shielding contour plots for ethane, in one of the  $\sigma_d$  symmetry planes (a), ethene, in the molecular plane (b) and in the vertical symmetry plane passing through the two carbons (d), ethyne, in one of the  $\sigma_v$  symmetry planes (c).  $\sigma_{\text{iso}}(\mathbf{r})$  in ppm, distances in Å.

So that we can compare the magnetic shielding picture of bonding in *s-trans*-1,3-butadiene to analogous descriptions of bonding in ethane, ethene and ethyne, we prepared  $\sigma_{\text{iso}}(\mathbf{r})$  contour plots in one of the  $\sigma_d$  symmetry planes in ethane [see Figure 6(a)], in the molecular plane and in the vertical symmetry plane passing through the two carbons in ethene [see Figure 6, (b) and (d), respectively], and in one of the  $\sigma_v$  symmetry planes in ethyne [see Figure 6(c)]. Clearly,

the sizes of the shielded areas between the carbons and the variations in shielding intensity within these areas are consistent with the expected differences between carbon-carbon single, double and triple bonds. Close examination of the  $\sigma_{\text{iso}}(\mathbf{r})$  contour plots in the molecular and vertical planes of *s-trans*-1,3-butadiene and ethane [see Figures 3(a) and 6(b), and 4(a) and 6(d), respectively] shows that the C–C “double” bond in *s-trans*-1,3-butadiene is weaker than the corresponding bond in ethene; the much weaker C–C “single” bond in *s-trans*-1,3-butadiene still bears more similarity to the C–C double bond in ethene than to the C–C single bond in ethane. There are no deshielded “halos” around the  $\text{sp}^3$  hybridized carbons in ethane [see Figure 6(a)]; the deshielded “halos” next to the  $\text{sp}$  hybridized carbons in ethyne are not only much smaller than those in ethene and *s-trans*-1,3-butadiene [*cf.* Figures 6(b–d), 3(a) and 4(a)], but also directed towards opposing carbons only, *i.e.* ethyne does not show deshielded areas along C–H bonds. It is well-known that, among ethane, ethene and ethyne, the most deshielded carbon nuclei are those in ethene, followed by ethyne and ethane (see, for example, the  $^{13}\text{C}$  absolute shielding scale<sup>19</sup>). This ordering can be explained by the differences between the close environments of the carbon nuclei in ethane, ethene and ethyne shown in Figure 6.

The  $\sigma_{\text{iso}}(\mathbf{r})$  contour plots for ethane, ethene, ethyne and *s-trans*-1,3-butadiene in Figures 6, 3(a) and 4(a) demonstrate that the state of the hybridization of the carbon atom has a pronounced influence on the shapes and intensities of the shielded areas over the bonds in which this atom participates. The isotropic shielding  $\sigma_{\text{iso}}(\mathbf{r})$  is a smooth function of the position vector  $\mathbf{r}$ , therefore the more extensive variations in  $\sigma_{\text{iso}}(\mathbf{r})$  caused by the presence of deshielded “halos” around  $\text{sp}^2$  hybridized carbons “squeeze” the shielded regions over the C–C and C–H bonds in which these atoms are involved, making these regions smaller and less shielded. To a lesser degree, this effect is also observed for the  $\text{sp}$  hybridized carbons in ethyne, where it impacts the C–C bond only. As a consequence, if one examines  $\sigma_{\text{iso}}(\mathbf{r})$  contour plots in the respective molecular planes only, the C–H bonds to  $\text{sp}^2$  hybridized carbons appear to be slightly weaker than those to  $\text{sp}^3$  and  $\text{sp}$  hybridized carbons. A quantitative comparison between C–H bonds to  $\text{sp}^3$ ,  $\text{sp}^2$  and  $\text{sp}$  hybridized carbons would require an analysis of the shielding intensities within the volumes surrounding these bonds using three-dimensional  $\sigma_{\text{iso}}(\mathbf{r})$  data such as the GAUSSIAN cube file used to plot the  $\sigma_{\text{iso}}(\mathbf{r}) = \pm 16$  ppm isosurfaces shown in Figure 1(a).

A comparison between the isotropic shielding contour plots in the respective molecular planes for *s-trans*-1,3-butadiene, ethene, benzene,<sup>12</sup> five-membered heterocycles with one

heteroatom (furan, pyrrole, and thiophene)<sup>13</sup> and heterocycles with two heteroatoms (oxazole, imidazole, and thiazole)<sup>14</sup> shows a remarkable signature-like consistency in the magnetic shielding variations around  $sp^2$  carbons and over the bonds in which these atoms are involved. This is an indication that the magnetic shielding picture of chemical bonding is transferrable between molecules.

### 3. CONCLUSIONS

The comparison between the computed isotropic shielding and total electron density isosurfaces and contour plots for *s-trans*-1,3-butadiene reported in this paper demonstrates that studying the changes in isotropic shielding in the space surrounding a molecule provides a promising way of looking at chemical bonding, in which features just hinted in total electron density plots are shown much more clearly, amplified in a manner consistent with chemical intuition. Isotropic shielding, just as the total electron density, shows details of all bonds in a molecule, in this particular case, of all C–C and C–H bonds, without separating the C–C bonds into  $\sigma$  and  $\pi$  components. Due to the partial character of the carbon-carbon “single” and “double” bonds in *s-trans*-1,3-butadiene, exposing the differences between these bonds is more difficult than doing so for a molecule with isolated single and double bonds; distinguishing between the three symmetry-unique C–H  $\sigma$  bonds which are very similar in strength is an equally challenging task. If the aim is to characterize bonds using single numbers, bond-orders from simple HMO theory (for the C–C bonds) or alternative all-electron approaches<sup>20,21</sup> may provide reasonable estimates of relative bond strengths, but if we want to investigate the spatial extents of the bonds and the way in which bonding interactions vary around bonds, the total electron density plots are often not particularly helpful. The information about chemical bonding carried by the total electron density can be enhanced by calculating and examining its gradient and Laplacian; an example is provided by Bader’s Quantum Theory of Atoms in Molecules (QTAIM);<sup>22</sup> additional details can be obtained through a domain-averaged Fermi hole (DAFH) analysis.<sup>23</sup> Other approaches used to analyze chemical bonding employ more complicated descriptors: The electron localization function (ELF)<sup>24</sup> and the localized orbital locator (LOL)<sup>25</sup> involve the kinetic energy density, the total electron density and its gradient (for a recent review of these and other methods that can be used to analyze “fuzzy” chemical concepts, such as the chemical bond, see Ref. 26). In contrast, as shown by our results for *s-trans*-1,3-butadiene, the isotropic

shielding isosurfaces and contour plots provide high levels of detail about chemical bonding directly, without a need to construct additional more complicated descriptors. Further advantages of an analysis based on the isotropic shielding are that it has a straightforward physical interpretation and, just as the total electron density, is underpinned by experimentally measurable quantities (nuclear shieldings).

The isotropic shielding contour plots for ethane, ethene and ethyne illustrate very well the differences between carbon-carbon single, double and triple bonds; even visual comparison between the plots for ethene and *s-trans*-1,3-butadiene is sufficient to show that the ethene carbon-carbon bond is stronger than the “double” bond in *s-trans*-1,3-butadiene. The differences between the close surroundings of the  $sp^3$ ,  $sp^2$  and  $sp$  hybridized carbons in ethane, ethene and ethyne can be linked to the experimental observation<sup>19</sup> that the most deshielded carbon nuclei are those in ethene, followed by ethyne and ethane. This is the first indication that the deshielded “halos” around  $sp^2$  and  $sp$  hybridized carbons observed initially in benzene and cyclobutadiene<sup>12</sup> relate to experimentally measurable NMR properties.

The computational costs associated with calculating grids of isotropic shielding values are higher than those needed for evaluating the total electron density. However, for a number of molecules it will be sufficient to use the relatively cheap HF-GIAO method. It is well-known that accurate nuclear shielding calculations require extended basis sets; the same applies to NICS, if these are used to compare molecules exhibiting similar levels of aromaticity.<sup>13</sup> In our experience, the magnetic shielding variations over bonds are less affected by the quality of the basis set used in the calculations and smaller basis sets, such as 6-31+G(d) or even 6-31G(d), can produce pictures which show more significant differences from those shown in Figures 1, 2–6 only within the regions close to the nuclei.

In principle, once data about the isotropic shielding distribution around a molecule are available, this distribution can be partitioned using any method that can be applied to the total electron density, for example, QAIM,<sup>22</sup> or Hirshfeld’s approach,<sup>27</sup> with the restriction that, for now, derivatives need to be numerical rather than analytical.

## **AUTHOR INFORMATION**

### **Corresponding Author**

\*peter.karadakov@york.ac.uk

## Notes

The authors declare no competing financial interests.

## ACKNOWLEDGMENTS

The authors thank the Department of Chemistry of the University of York for a Teaching Scholarship to K.E.H.

## References

- (1) Johnson, C. E.; Bovey, F. A. *J. Chem. Phys.* **1958**, *29*, 1012–1014.
- (2) Schleyer, P. v. R.; Maerker, C.; Dransfeld, A.; Jiao, H.; Hommes, N. J. R. v. E. *J. Am. Chem. Soc.* **1996**, *118*, 6317–6318.
- (3) Cernusak, I.; Fowler, P. W.; Steiner, E. *Mol. Phys.* **2000**, *98*, 945–953.
- (4) Schleyer, P. v. R.; Manoharan, M.; Wang, Z. X.; Kiran, B.; Jiao, H.; Puchta, R.; Hommes, N. J. R. v. E. *Org. Lett.* **2001**, *3*, 2465–2468.
- (5) Steiner, E.; Fowler, P. W.; Jenneskens, L. W. *Angew. Chem. Int. Ed.* **2001**, *40*, 362–366.
- (6) Fallah-Bagher-Shaidaei, H.; Wannere, C. S.; Corminboeuf, C.; Puchta, R.; Schleyer, P. v. R. *Org. Lett.* **2006**, *8*, 863–866.
- (7) Wolinski, K. *J. Chem. Phys.* **1997**, *106*, 6061–6067.
- (8) Klod, S.; Kleinpeter, E. *J. Chem. Soc., Perkin Trans. 2* **2001**, 1893–1898.
- (9) Kleinpeter, E.; Klod, S.; Koch, A. *J. Mol. Struct. THEOCHEM* **2007**, *811*, 45–60.
- (10) Kleinpeter, E.; Koch, A. *Phys. Chem. Chem. Phys.* **2012**, *14*, 8742–8746.
- (11) Kleinpeter, E.; Koch, A. *J. Phys. Chem. A* **2012**, *116*, 5674–5680.
- (12) Karadakov, P. B.; Horner, K. E.; *J. Phys. Chem. A* **2013**, *117*, 518–523.
- (13) Horner, K. E.; Karadakov, P. B. *J. Org. Chem.* **2013**, *78*, 8037–8043.
- (14) Horner, K. E.; Karadakov, P. B. *J. Org. Chem.* **2015**, *80*, 7150–7157.
- (15) Frisch, M. J.; Trucks, G. W.; Schlegel, H. B.; Scuseria, G. E.; Robb, M. A.; Cheeseman, J. R.; Scalmani, G.; Barone, V.; Mennucci, B.; Petersson, G. A.; Nakatsuji, H.; Caricato, M.; Li, X.; Hratchian, H. P.; Izmaylov, A. F.; Bloino, J.; Zheng, G.; Sonnenberg, J. L.; Hada, M.; Ehara, M.; Toyota, K.; Fukuda, R.; Hasegawa, J.; Ishida, M.; Nakajima, T.; Honda, Y.; Kitao, O.; Nakai, H.; Vreven, T.; Montgomery, J. A., Jr.; Peralta, J. E.; Ogliaro, F.; Bearpark, M.; Heyd, J. J.; Brothers, E.; Kudin, K. N.; Staroverov, V. N.; Keith, T.;

- Kobayashi, R.; Normand, J.; Raghavachari, K.; Rendell, A.; Burant, J. C.; Iyengar, S. S.; Tomasi, J.; Cossi, M.; Rega, N.; Millam, N. J.; Klene, M.; Knox, J. E.; Cross, J. B.; Bakken, V.; Adamo, C.; Jaramillo, J.; Gomperts, R.; Stratmann, R. E.; Yazyev, O.; Austin, A. J.; Cammi, R.; Pomelli, C.; Ochterski, J. W.; Martin, R. L.; Morokuma, K.; Zakrzewski, V. G.; Voth, G. A.; Salvador, P.; Dannenberg, J. J.; Dapprich, S.; Daniels, A. D.; Farkas, O.; Foresman, J. B.; Ortiz, J. V.; Cioslowski, J.; Fox, D. J. *Gaussian 09*, Revision D.01; Gaussian, Inc.: Wallingford, CT, 2013.
- (16) Craig, N. C.; Groner, P.; McJean, D. C. *J. Phys. Chem. A* **2006**, *110*, 7461–7469.
- (17) Hehre, W. J.; Radom, L.; Schleyer, P. v. R.; Pople, J. A. *Ab Initio Molecular Orbital Theory*; Wiley: New York, 1986, p. 147.
- (18) See [http://www.gaussian.com/g\\_tech/g\\_ur/u\\_cubegen.htm](http://www.gaussian.com/g_tech/g_ur/u_cubegen.htm).
- (19) Jameson, A. K.; Jameson, C. J. *Chem. Phys. Lett.* **1987**, *134*, 461–466.
- (20) Wiberg, K. B. *Tetrahedron* **1968**, *24*, 1083–1096.
- (21) Mayer, I. *Chem. Phys. Lett.* **1983**, *97*, 270–274.
- (22) Bader, R. F. W. *Atoms in Molecules: A Quantum Theory*; Oxford University Press: Oxford, 1990.
- (23) Ponec, R.; Cooper, D.L.; Savin, A. *Chem. Eur. J.* **2008**, *14*, 3338–3345.
- (24) Becke, A. D.; Edgecombe, K. E. *J. Chem. Phys.* **1990**, *92*, 5397–5403.
- (25) Schmider, H. L.; Becke, A. D. *J. Mol. Struct. THEOCHEM* **2000**, *527*, 51–61.
- (26) Gonthier, J. F.; Steinmann, S. N.; Wodrich, M. D.; Corminboeuf, C. *Chem. Soc. Rev.* **2012**, *41*, 4671–4687.
- (27) Hirshfeld, F. L. *Theor. Chem. Acc.* **1977**, *44*, 129–138.

---

for Table of Contents use only

Exploring Chemical Bonds through Variations in Magnetic Shielding

Peter B. Karadakov and Kate E. Horner

